

# Augmented Reality Enabled by On-Chip Meta-Holography Multiplexing

Yangyang Shi, Chengwei Wan, Chenjie Dai, Zejing Wang, Shuai Wan, Guoxing Zheng, Shuang Zhang, and Zhongyang Li\*

The exploit of on-chip metasurfaces with full optical controllability and multiplexing capability holds great promise for photonic integration circuits (PIC). Despite previous endeavors in metasurfaces controlling guided waves, it still faces critical challenges to realize practical display applications, for instance, augmented reality (AR). Here, a new type of AR based on multiplexed on-chip meta-holography is proposed and experimentally demonstrated by integrating judiciously engineered meta-atoms above waveguide. Through hybridizing detour and Pancharatnam–Berry phases, on-chip metasurfaces can independently manipulate both guided waves and free-space light to enable a triple-channel holography-multiplexing with independent-encoding freedom. Eventually, an RGB-coloring AR hologram free from zero-order diffraction that can project virtual images into a real-world environment is realized, showcasing its significant potential for wearable devices (glasses or contact lens) integration. This study finds a feasible route toward multifunctional PIC devices and applications in wearable AR displays, imaging multiplexing, information storage, etc.

## 1. Introduction

Photonic integrated circuits (PIC) provide an attractive and powerful platform for optical information processing<sup>[1]</sup> and augmented reality (AR) devices.<sup>[2–4]</sup> However, conventional PIC devices based on optical waveguides are usually bulky and lack the full control at the subwavelength-scale to achieve arbitrary

wavefront-shaping functionalities. Therefore, on-chip miniaturized devices capable of both on-chip and free-space wave manipulation are highly desired. Metasurfaces, ultrathin structured optical surfaces with unprecedented capability in engineering phase, amplitude, and polarization state of light in the subwavelength scale,<sup>[5,6]</sup> provide a new playground for AR applications.

Typical metasurfaces manipulate light in the free-space to achieve various applications including beam-steering,<sup>[7–9]</sup> metalens,<sup>[10]</sup> nanoprining display,<sup>[11,12]</sup> and meta-holography.<sup>[13–16]</sup> Recently, progress has been made on on-chip metasurfaces integrated with waveguide or supporting the surface plasmonic polaritons (SPP) modes that exhibit various functionalities, including guided-mode-conversion,<sup>[17,18]</sup> polarization beam-splitter,<sup>[19]</sup> directional emitters/couplers,<sup>[20–23]</sup> on-chip

metalens,<sup>[24–27]</sup> and meta-holography.<sup>[28]</sup> For instance, out-of-plane holography-multiplexing has been demonstrated based on on-chip metasurface with SPP excitations along different directions,<sup>[29]</sup> which significantly increases the information channel capacity. In addition to SPP, on-chip metasurface integrated with dielectric waveguide has been employed to realize light steering,<sup>[30]</sup> meta-focusing,<sup>[31–33]</sup> orbital angular momentum generation,<sup>[34]</sup> and holography-multiplexing<sup>[35,36]</sup> with the improved image quality and efficiency. The integration of metasurface with optical waveguides provides a new route to facilitate chip-scale photonic systems to more practical fields.

Despite these previous endeavors,<sup>[37,38]</sup> on-chip metasurfaces still face the critical challenge to create practical AR devices in real life. Most on-chip metasurface architectures depend on SPP propagation or reflective substrate to strongly confine the guiding waves, which makes the meta-device optically opaque and cannot enable AR. Besides, the projected image from surface waves is often overwhelmed by the background light and hardly resolved due to the low diffraction efficiency. Moreover, multiplexing capability remains unexplored to achieve independent multichannel displays that can alternatively operate in free-space or on-chip modes.


Here, we propose and experimentally realize a new type of miniaturized AR hologram device by using on-chip metasurfaces to enable RGB-coloring holography-multiplexing

Y. Shi, C. Wan, C. Dai, Z. Wang, S. Wan, G. Zheng, Z. Li  
Electronic Information School  
Wuhan University  
Wuhan 430072, China  
E-mail: zhongyangli@whu.edu.cn

G. Zheng, Z. Li  
Wuhan Institute of Quantum Technology  
Wuhan 430206, China

G. Zheng, Z. Li  
School of Microelectronics  
Wuhan University  
Wuhan 430072, China

S. Zhang  
Department of Physics  
The University of Hong Kong  
Pokfulam Road, Hong Kong 999077, China

 The ORCID identification number(s) for the author(s) of this article can be found under <https://doi.org/10.1002/lpor.202100638>

DOI: 10.1002/lpor.202100638

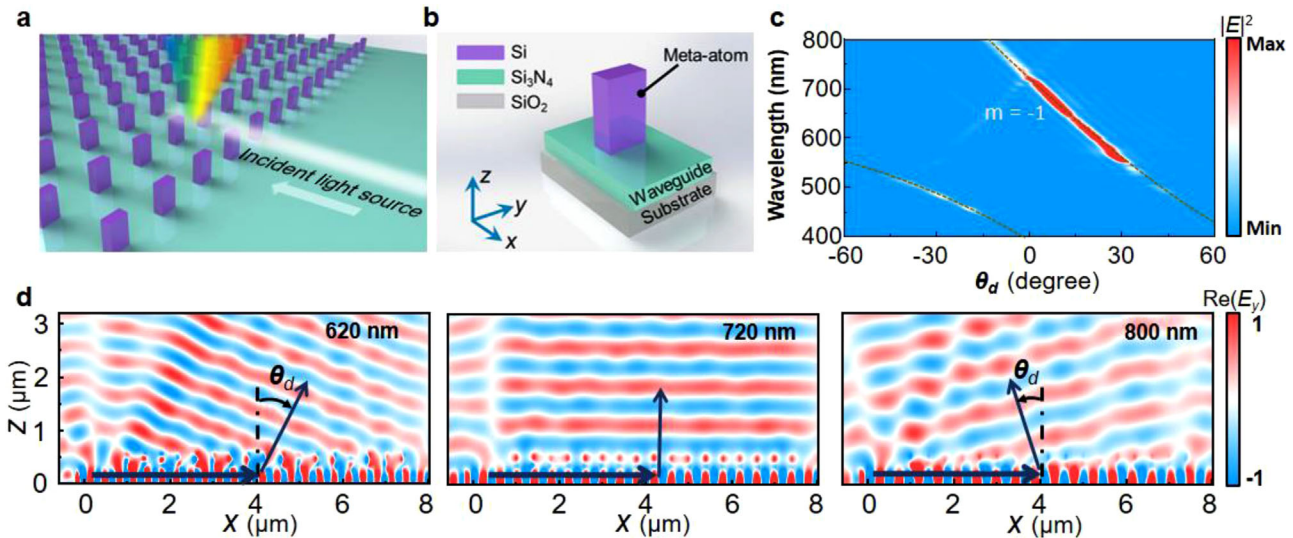


**Figure 1.** On-chip metasurface mechanism for beam-steering. a) Schematic of guided wave extraction and beam-steering with on-chip metasurface. The metasurface consists of an array of periodically distributed meta-atoms. b) Schematic of  $\alpha$ -Si nanoblock on top of a  $\text{Si}_3\text{N}_4$  waveguide and  $\text{SiO}_2$  substrate. c) Simulated far-field intensity  $|E|^2$  as a function of deflection angles  $\theta_d$  (x-axis) and wavelength (y-axis). d) Calculated electric-field profiles ( $E_y$ ) and wavefronts of the extracted light from the on-chip metasurface driven by propagating guided waves along the x-direction at the wavelength of 620, 720, and 800 nm, respectively. The steering directions of the extracted light are denoted by the arrows.

functionality. Through the integration of judiciously engineered meta-atoms onto the waveguide, the on-chip propagating waves along the planar waveguide can be efficiently emitted into free-space and molded into any arbitrary wavefronts. Utilizing the spatial degrees of freedom of the antennas to induce the two-dimensional detour phase, a dual-channel meta-holography with independent-encoding freedom is realized and experimentally captured as a colorful AR hologram. Moreover, by combining the on-chip detour phase with the free-space Pancharatnam–Berry (PB) phase, the on-chip metasurface simultaneously manipulates both the on-chip guided and the free space light waves, thus extending the multiplexing functionalities for both in-plane and out-of-plane modes. It expands the AR multiplexing to triple-channel to independently exhibit RGB-coloring images, which goes beyond the state-of-art of meta-holography based only on waveguide. Compared with free-space holography, the projected images here are free from the zero-order diffraction interference to the observer due to the optical on-chip propagation scheme. Therefore, the proposed on-chip AR hologram has the potential to be integrated with eyeglasses or contact lens and projects the virtual image to interact with the real-world environment. Benefitting from on-chip integration, device miniaturization, and high capacity in multiplexing, we envision that the AR technology from on-chip metasurface will usher in next-generation wearable AR displays, multiplexing optical display, information storage, remote sensing, etc.

## 2. Results and Discussion

### 2.1. On-Chip Metasurfaces for Beam-Steering

In contrast to the designs of metasurfaces for free-space light interaction, the on-chip metasurface is patterned and integrated on top of an optical waveguide. The incident light is coupled into

the guided mode and is subsequently modulated and reradiated by the judiciously engineered meta-atoms, as shown in **Figure 1a**. Here, the metasurface consists of amorphous silicon ( $\alpha$ -Si) nanoblock arrays on top of a planar waveguide of  $\text{Si}_3\text{N}_4$  (thickness = 220 nm) with a high effective index  $n \approx 2.05$ , as shown in **Figure 1b**, in which a relatively thick ( $\approx 500 \mu\text{m}$ ) layer of silica serves as the bottom cladding substrate. The simulated electric-/magnetic-field distributions above the waveguide can be found in **Figure S2**, Supporting Information, which shows the coupling of guided mode back to the free space radiation.

In contrast to the geometrical parameters changes of shape, size, and rotation angle in conventional free-space metasurface design, our phase arrangement depends on the detour phase that is determined by the meta-atoms' relative locations.<sup>[6,15,39]</sup> The essence of the on-chip metasurface is to arrange the meta-atoms to couple and mold the guided waves into arbitrary wavefronts back into the free-space. The detour phase for the extracted light by meta-atoms is expressed as (more details can be found in Section S1, Supporting Information):

$$\Delta\phi_m(x) = \frac{2\pi}{\Lambda} \cdot \Delta x_m \quad (1)$$

$$\Delta\phi_n(y) = \frac{2\pi}{\Lambda} \cdot \Delta y_n \quad (2)$$

where  $\Delta x_m$  and  $\Delta y_n$  are the  $m_{\text{th}}$  and  $n_{\text{th}}$  meta-atom displacement along x- and y-directions within a period of  $\Lambda$ , respectively. For periodically distributed meta-atoms on top of the waveguide, the exhibited beam-steering functionality is similar to the meta-grating.<sup>[8,37]</sup> The output angle of the extracted wave is expressed as (Section S2, Supporting Information):

$$\theta_d = \sin^{-1} \left( n_{\text{eff}} + \frac{m\lambda_0}{\Lambda} \right) \quad (3)$$

where  $n_{\text{eff}}$  is the effective refractive index of the waveguide mode, and  $\lambda_0$  is the free-space wavelength, respectively. Here, the propagation constant is  $\beta = 2\pi \cdot n_{\text{eff}} / \lambda_0$ , which can be numerically retrieved for the fundamental TE<sub>0</sub> mode at different wavelengths. According to Equation (3), for a fixed propagation constant  $\beta$  of a given wavelength, the diffraction angle of the outgoing beam is determined by the array period. Figure 1c plots the far-field intensity  $|E|^2$  as a function of the deflection angle and wavelength of the outgoing beam. It is observed that the guided wave is coupled into free-space with a well-defined angle of the diffraction order ( $m = -1$ ). The higher-order diffraction mode is weak and can be negligible. Specifically, the calculated electric-field profiles (Figure 1d) illustrate that the diffraction angle at the wavelengths of 620, 720, and 800 nm are, respectively,  $\approx 19^\circ$ ,  $\approx 1^\circ$ , and  $\approx -12^\circ$ . Note that the beam-steering performance can be regarded as a particular wavefront shape or holographic distribution at the far-field. Therefore, moving forward to further enable AR hologram, the demonstrated beam-steering functionality would serve as the fundamental mechanism through strategically distributing the meta-atoms along the waveguide and extracting the guided waves with elaborate phase design.

## 2.2. On-Chip Meta-Holography

Consequently, based on the encoding-freedom from detour phases, it is possible to generate arbitrary wavefront by strategically designing the meta-atom locations, where the scattering phase for each meta-atom is decided by the relative displacement within a period. Note that the propagating guided waves along the  $x$ - and  $y$ -directions would acquire completely independent scattering phases, according to Equations (1) and (2). Based on such independent detour phases along orthogonal dimensions, we demonstrate a simple way to display dual-channel meta-holographic images based on a single on-chip metasurface, as shown in Figure 2a. Here, the guided waves propagating along  $x$ - and  $y$ -directions are, respectively, scattered by the on-chip metasurface to form colorful meta-holographic images of “Red Flower” and “Green Leaf” in free space. Figure 2b,c shows the distributed array and design guideline for the on-chip metasurface.  $P_x$  and  $P_y$  are the periods of the unit cell along  $x$ - and  $y$ -directions, which are determined by the wavelengths of the incident guided waves. The width  $W$  and length  $L$  of the  $\alpha$ -Si nanoblock is 90 nm and its height is 380 nm. For TE<sub>0</sub> mode, the detour phases generated from each nanoblock along  $x$ - or  $y$ -direction are determined by the meta-atom displacement of  $\Delta x$  and  $\Delta y$ , as denoted in Figure 2b. Hence, the on-chip metasurface array is designed by a mapping from the designed detour phases.

The sample fabrication starts with the deposition of the Si<sub>3</sub>N<sub>4</sub> waveguide film on top of the silica substrate by plasma-enhanced chemical vapor deposition (PECVD). The on-chip metasurface is patterned on an  $\alpha$ -Si layer grown by PECVD and electron-beam lithography (EBL), as shown in the scanning electron microscopy (SEM) image (Figure 2d). The fabricated array consists of  $900 \times 900$  meta-atoms with an area size of  $315 \times 270 \mu\text{m}^2$ . More detailed discussion for the fabrication processing can be found in Experimental Section and Figure S4, Supporting Information. The experimental setup for hologram characterization is schematically shown in Figure 2e. The polar-

ized laser source is coupled into the on-chip waveguide through wide-oblique illumination from the sample edge and Camera 1 is utilized to capture the hologram projected to the optically opaque screen. By rotating the sample to illuminate the light source from the other direction, the other channel of detour phase can be triggered and captured. Figure 2f shows the designed phase arrangement and the holographic image, which is in good agreement with the simulation result calculated with Gerchberg–Saxton algorithm by MATLAB. Specifically, “Red Flower” is obtained by a TE<sub>0</sub> guided wave at 650 nm propagating along  $x$ -direction, while “Green Leaf” is reconstructed by the guided wave at 560 nm along  $y$ -direction. More experimental images for a broad range of wavelengths can be found in Experimental Section and Figure S6, Supporting Information.

## 2.3. Multichannel Meta-Holography from On-Chip and Free-Space Multiplexing

To gain more multiplexing capacity, we further demonstrate a new strategy to combine the on-chip dual-dimensional detour phase with the extra degree of encoding-freedom for free-space modulation, as shown in Figure 3a–d. The combination of the on-chip detour phases in Figure 3a and the geometric phase (PB) in Figure 3b results in the hybrid phase arrangement in Figure 3c, with a zoom-in view of the nanoblock in Figure 3d. Note that each meta-atom orientation provides the PB phase modulation for free space light while its displacement controls the detour phase for the scattering of the guided mode. Hence, there are enough degrees of freedom for achieving triple-channel holography-multiplexing (Figure 3e) with improved information capacity. Specifically, the TE<sub>0</sub> guided waves at 560 or 480 nm along  $x$ -/ $y$ -directions are scattered by the metasurface to form two independently encoded holographic images, namely, the green letter “G” and the blue letter “B,” respectively. Meanwhile, the on-chip metasurface also projects a third-channel holographic image of the red-color letter “R” based on the PB phase under the direct illumination of left circular polarized light at 650 nm. The SEM image of the fabricated sample and the optical setup for characterization of the sample are shown in Figures 3f and 3g, respectively. Owing to the triple-channel holography being independent from each other, here we employ a single laser source with tunable wavelength to illuminate the sample from different directions for a proof-of-concept demonstration. Different holographic images are, respectively, reconstructed by illumination from either edge oblique coupling scheme (same as Figure 2e) or incidence from free-space. Here, the triple-channel holography is demonstrated with both monochromatic and multiwavelength schemes. Figure 3h shows the excellent agreement between the simulated (via MATLAB) and experimental holographic images. Specifically, the monochromatic holographic letters “W,” “H,” and “U” (the abbreviation represents Wuhan University) are well captured by Camera 1 on the optically opaque screen under different illumination schemes. In addition, another triple-channel colorful holography is demonstrated with the projected letters “R,” “G,” and “B” under the guided and free-space illumination from  $x$ -/ $y$ -/ $z$ -directions, respectively. Overall, such hybrid holography-multiplexing based on on-chip/free-space excitations is switchable to display independent-channel imaging with

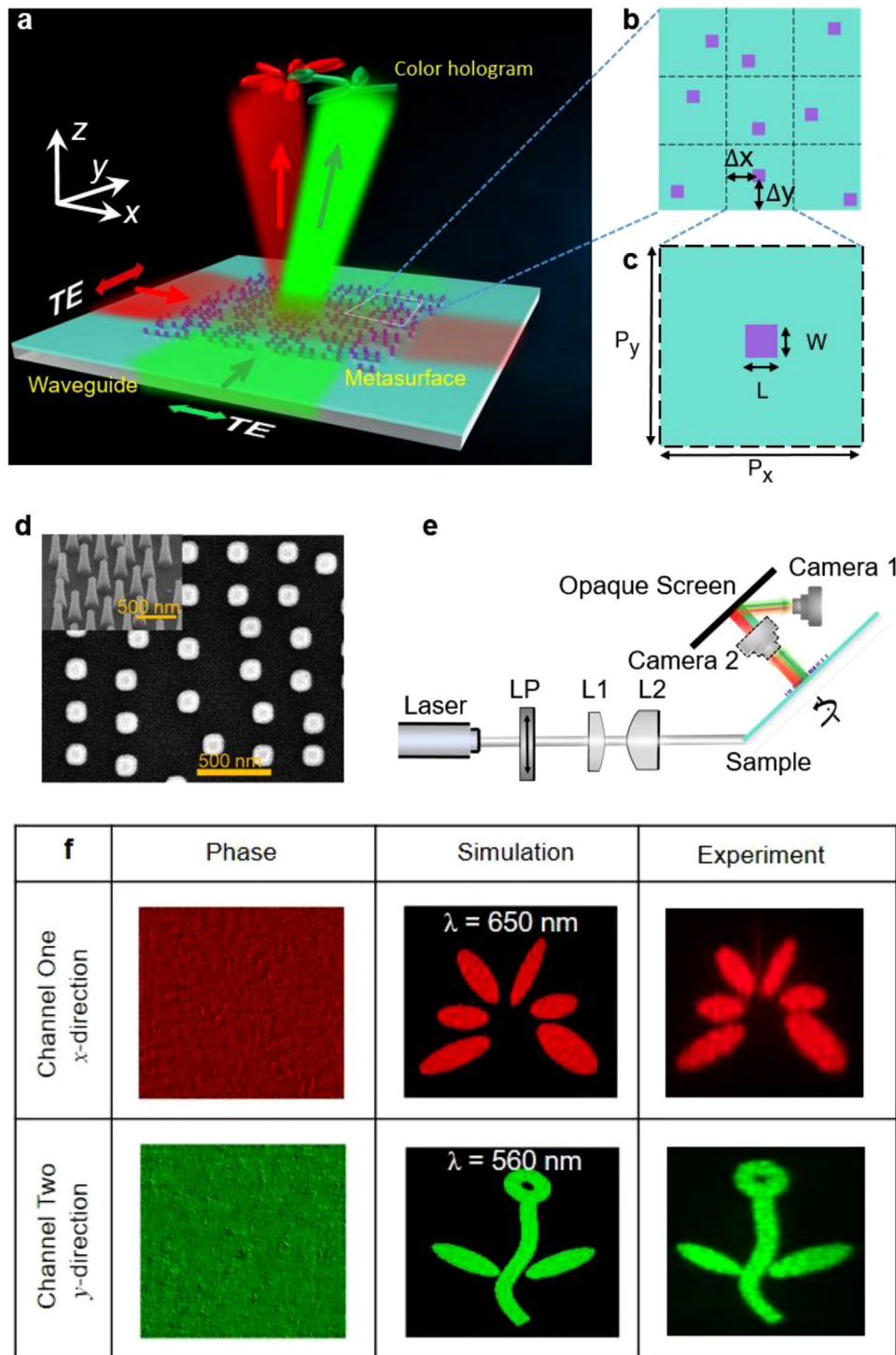


**Figure 2.** Dual-channel on-chip meta-holography. a) Schematic for the propagating waves in the slab waveguide being extracted to project a coloring holographic image (“Red Flower” + “Green Leaf”) in free space. b) Top-view of the selected metasurface region and c) the unit cell. The corresponding geometric parameters are  $P_x = 350 \text{ nm}$ ,  $P_y = 300 \text{ nm}$ , and  $L = W = 90 \text{ nm}$ . d) SEM image for the fabricated metasurface sample. e) Optical measurement setup for observing dual-channel holography images. f) Simulated and measured meta-holographic phases/images. The holographic images of “Red Flower” and “Green Leaf” are displayed for the  $TE_0$  modes incidence from x- and y-directions at the wavelengths of 650 and 560 nm, respectively.



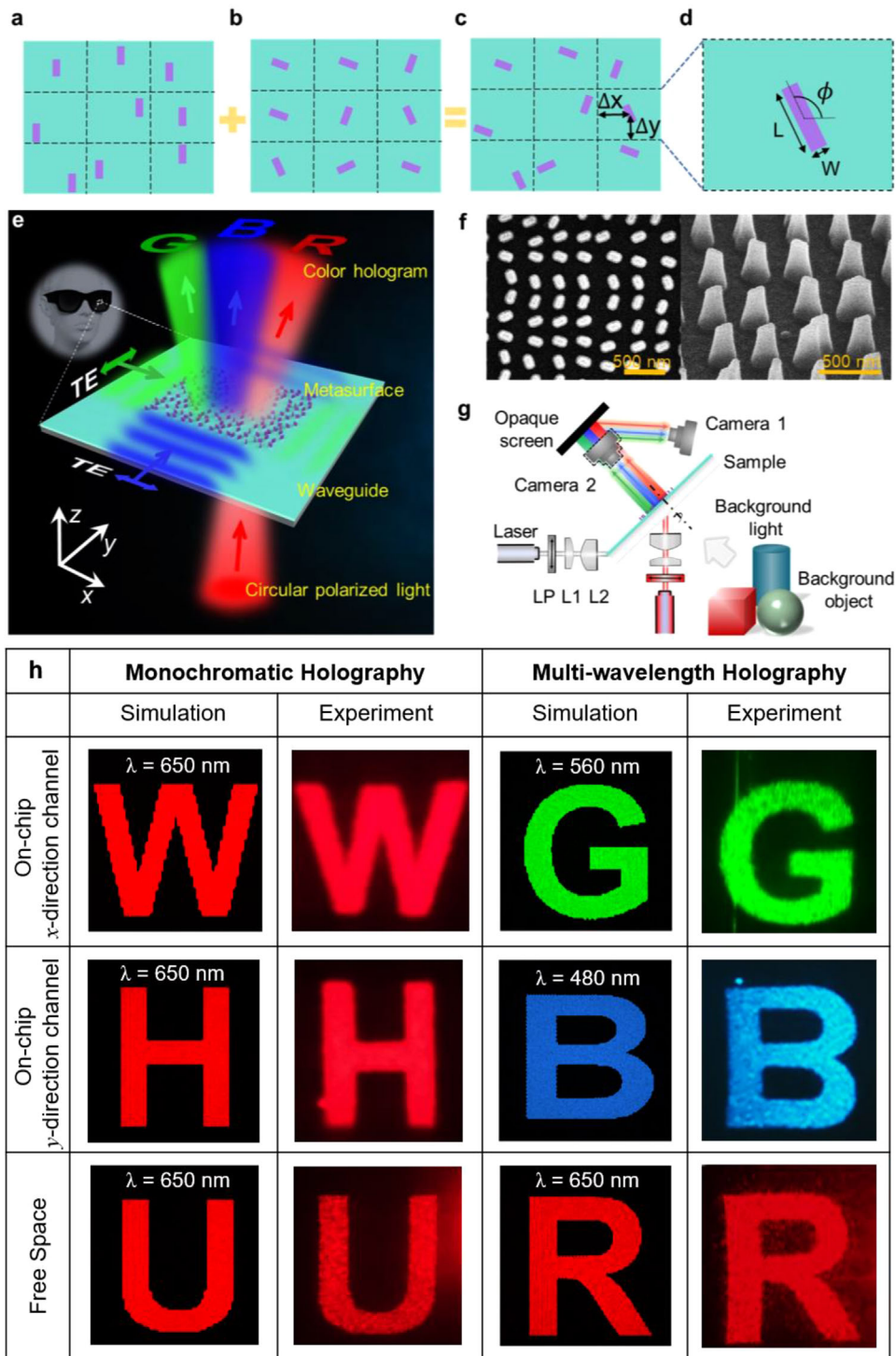


**Figure 3.** Triple-channel meta-holography multiplexing from both on-chip detour phase and free-space PB phase. a) The metasurface array relying on on-chip detour phase encoding and b) conventional free-space metasurface with PB phase. c) The proposed triple-channel holographic metasurface by hybridizing (a) and (b) with d) the zoom-in unit cell. The detour displacement  $\Delta x/\Delta y$  and the orientation angle  $\phi$  are independently encoded. e) Conceptual illustration for triple-channel multiplexed meta-holography. f) SEM image of the fabricated sample. g) Optical experimental setup for the triple-channel holography characterization. h) Simulated and measured monochromatic ("W," "H," and "U") and multiwavelength ("R," "G," and "B") holographic images for the guided waves and free-space light incidence from x-/y-/z-direction. The geometric parameters of the optimized nanoblock to reconstruct the holographic letters "W," "H," and "U" are  $P_x = P_y = 350 \text{ nm}$ ,  $L = 140 \text{ nm}$ ,  $W = 70 \text{ nm}$ , and the height is  $380 \text{ nm}$ . The geometric parameters of the optimized nanoblock to reconstruct the holographic letters "R," "G," and "B" are  $P_x = 300 \text{ nm}$ ,  $P_y = 250 \text{ nm}$ ,  $L = 130 \text{ nm}$ ,  $W = 60 \text{ nm}$ , and the height is  $380 \text{ nm}$ .

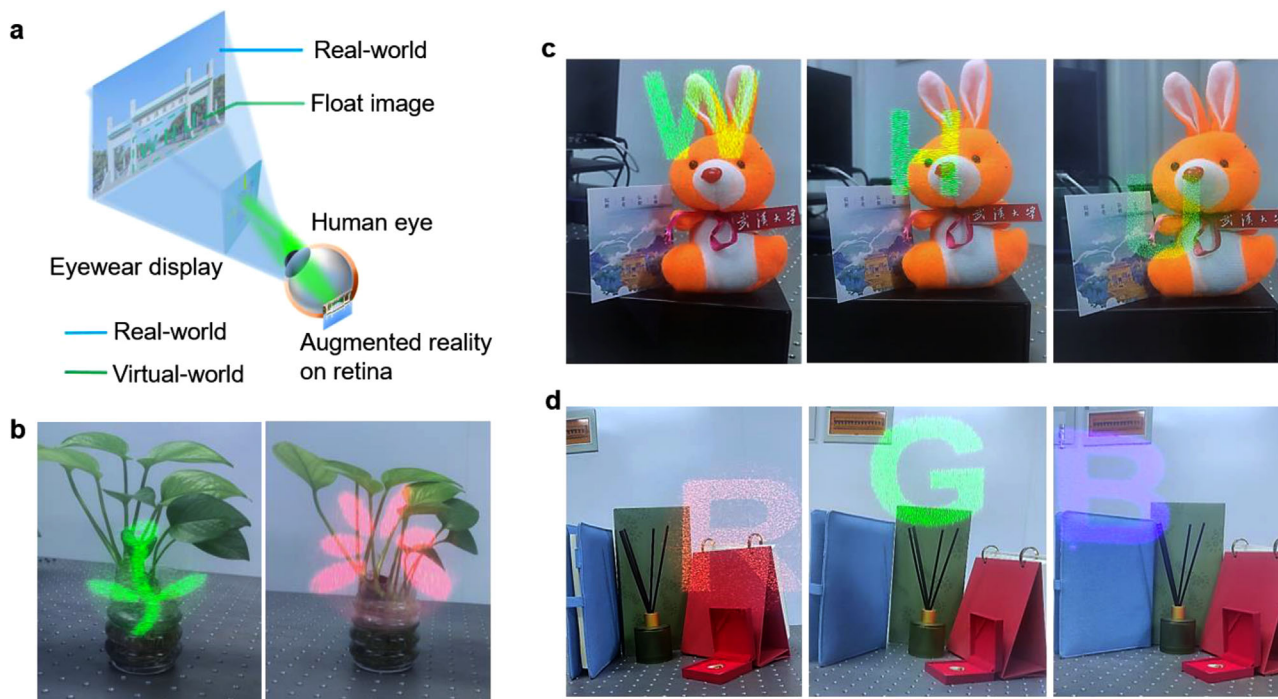


**Figure 4.** AR demonstration by the proposed on-chip metasurfaces. a) Conceptual illustrations of the AR hologram system by on-chip metasurface devices. b) AR imaging display from dual-channel on-chip meta-holography to exhibit images of “Red Flower” or “Green Leaf” floating on top of a real plant scene. c) AR imaging displays to show the mixture of a real-world scene and the floating letters “W,” “H,” and “U.” d) AR imaging to show with colorful letters “R,” “G,” and “B” floating around real objects with corresponding colors at three different wavelengths (620, 532, and 460 nm).

minimum crosstalk. In contrast to the conventional free-space metasurface, our on-chip metasurface defined here refers to nanostructure arrays integrated onto the optical waveguide. Note that it can purely work as “in-plane” mode as shown in Figure 2. In the meanwhile, it can also operate in the hybrid mode of both “in-plane” and “out-plane,” as shown in Figure 3.

Although the fabricated nanostructures are slightly tapered (Figures 2d and 3f), it experimentally exhibits a quite clear holographic image as shown in Figures 2f and 3h (more details can be found in Section S7, Supporting Information). Here, the measured efficiency of the on-chip channel holography is defined as the ratio of the optical power projected into holography, to the optical power encountering with the holographic pattern area, which is experimentally measured to be  $\approx 3\%$ . In addition, the measured efficiency of free-space channel holography is defined as the ratio of the holographic power (calculated by the total transmitted light subtracting the zero-order component) to the total input optical power, which is experimentally measured to be  $\approx 7\%$ . Despite that the measured efficiency is not high, it is enough for the AR hologram application and practically observing the AR image, as shown in Figure 4.

## 2.4. Miniaturized RGB-Coloring AR Hologram

Finally, we demonstrate the practical holography-multiplexing AR functionality based on on-chip metasurfaces capable of projecting the floating holographic images in the real-world environment. As one of the most significant and promising technol-

ogy in display and imaging, AR serves to overlay virtual information with the real world, thus providing humans with an actual immersive experience. Due to the all-dielectric architecture with good transparent property and interference free from zero-order diffraction to the observer, our on-chip metasurface can be integrated with eyewear devices (for instance, eyeglasses or contact lens) for AR, as conceptually illustrated in Figure 4a.

Here we capture the sight view of the floating virtual information in the real-world environment by the camera in a mobile phone (Camera 2 in Figures 2e and 3g). As shown in Figure 4b, we clearly observe the actual sight view of “Red Flower” or “Green Leaf” floating on top of a real plant, with satisfactory imaging intensity, clarity, and sharpness. Compared with free-space holography, the projected images here are free from the zero-order diffraction interference to the observer due to the optical on-chip propagation scheme. Likewise, Figure 4c shows the triple-channel sight view of floating letters of “W,” “H,” and “U” in the real-world scene at a monochromatic wavelength of 532 nm. Figure 4d presents the sight-view of AR with colorful “R,” “G,” and “B” letters overlaying the corresponding colored objects in the real world. Corresponding experimental movies to exhibit the RGB-coloring AR hologram are Movies S1–S3, Supporting Information. Note that the free-space hologram channel here is off-axis illuminated by the laser source to avoid any influence from the zero-order beam, as shown in Figure 3g. Therefore, the projected free-space hologram and background objects can be simultaneously captured by Camera 2, thus generating the AR performance free from the zero-order beam influence.

The proposed AR strategy based on on-chip metasurfaces is compatible with current PIC technology and hence it can be readily integrated with wearable photonic devices, such as eyeglasses or contact lens.

### 3. Conclusion

In summary, we have proposed and demonstrated a new type of miniaturized AR hologram device with holography-multiplexing functionality based on on-chip metasurfaces. By incorporating the detour phase with free-space PB phase, a triple-channel hologram with independent-encoding freedom is demonstrated to simultaneously manipulate both the on-chip guided and the free-space light waves. Our approach effectively enhances the multiplexing capacity for storing information without increasing the complexity. Furthermore, compared with free-space holography, the projected images here are free from the zero-order diffraction interference to the observer due to the optical on-chip propagation scheme. Further works of dynamic control by incorporating tunable components such as liquid crystals and spatial light modulators would empower the on-chip meta-holography with the tuning capability. We envision that the proposed on-chip metasurface device with the advantage of miniaturization, multifunctionality, and broadband operation, can be applied in next-generation wearable AR displays, multiplexing optical display, information storage, remote sensing, etc.

### 4. Experimental Section

**Sample Fabrication:** The 220 nm thick layer of  $\text{Si}_3\text{N}_4$  waveguide was deposited on top of 500  $\mu\text{m}$  thick fused silica substrate by PECVD, and a 380 nm thick layer of  $\alpha$ -Si was consequently deposited onto the  $\text{Si}_3\text{N}_4$  waveguide via PECVD. To pattern the metasurface array, polymethyl methacrylate (PMMA) was spin-coated on  $\alpha$ -Si and baked at 150 ° for 3 min, and then a conductive polymer was also spin-coated to prevent charge accumulation. The sample was exposed by EBL (Raith 150, 20 kV) and subsequently developed in solution for 80 s. A chromium (Cr) layer of 20 nm thick as a dry-etch mask was deposited via thermal evaporation. After the PMMA resists were removed by lift-off process in acetone, the patterns of Cr hard mask were transferred to  $\alpha$ -Si by using reactive ion etching and then removed by Cr etchant. The holograms of “W,” “H,” and “U” were fabricated with the sample size of 315 × 315  $\mu\text{m}^2$  and composed of 900 × 900 meta-atoms. The coloring holograms of “R,” “G,” and “B” were fabricated with the sample size of 270 × 225  $\mu\text{m}^2$  and composed of 900 × 900 meta-atoms.

**Numerical Simulation:** Numerical simulations were implemented by using the finite-difference time-domain method (Figure 1c,d and Figures S2, S3, S5, and S7, Supporting Information). A structural model composed of an array of  $\alpha$ -Si nanoblocks placed on top of the  $\text{Si}_3\text{N}_4$  ( $n \approx 2.05$ ) waveguide and a glass substrate ( $n = 1.45$ ) was established. The guided waves of the transverse electric ( $\text{TE}_0$ ) mode propagated through the slab waveguide. The corresponding geometric parameters of the selected nanoblock in Figure 1 are  $P_x = 400$  nm,  $P_y = 300$  nm,  $L = 100$  nm,  $W = 180$  nm, and the height is 360 nm. Periodic boundary conditions for beam-steering or perfectly matched layers (PML) for

meta-holography were applied along  $y$ -direction and PMLs conditions for the  $x$ - and  $z$ -axis. For the hologram design and MATLAB simulation (Figures 2f and 3h), the Gerchberg–Saxton algorithm was utilized to obtain the required phase profile of the given images.

**Optical Measurement:** The on-chip meta-holography was characterized by utilizing the optical setup shown in Figure 2e. A linear polarizer was placed behind the laser light source and the combination of two lenses ( $L_1/L_3$  and  $L_2/L_4$ ) was used to collimate the beam. The polarized laser source was coupled into the on-chip waveguide by wide-oblique illumination from the sample edge. By rotating the sample to illuminate the light source from the other direction, the other channel of detour phase could be triggered and captured. The holographic images projected on the optically opaque screen could be observed directly or collected by an imaging Camera 1 (same as Camera 1 in Figure 3g). For the optical characterization of triple-channel meta-holography, the authors utilized the scheme shown in Figure 3g by simultaneously adding the 650 nm laser to directly illuminate the sample surface to generate the third-channel holography. As for the AR hologram, the sight view of the floating virtual information in the real-world environment was captured by a mobile phone (Camera 2 in Figures 2e and 3g).

### Supporting Information

Supporting Information is available from the Wiley Online Library or from the author.

### Acknowledgements

Y.S. and C.W. contributed equally to this work. The authors gratefully acknowledge Hubei Province Funds for Distinguished Young Scientists (2021CFA043), Wuhan Science and Technology Bureau (2020010601012196), Recruitment Program of Global Experts (501100010871), Start-up Program of Wuhan University (501100007046), and the Hong Kong Research Grant Council (AoE/P-502/20, 17309021). The work was supported by the Center for Nanoscience and Nanotechnology at Wuhan University and Hubei Luojia Laboratory.

### Conflict of Interest

The authors declare no conflict of interest.

### Data Availability Statement

The data that support the findings of this study are available from the corresponding author upon reasonable request.

### Keywords

augmented reality, meta-holography, multiplexing, on-chip metasurfaces, waveguides

Received: November 9, 2021

Revised: March 15, 2022

Published online:

- [1] Z. Xie, T. Lei, F. Li, H. Qiu, Z. Zhang, H. Wang, C. Min, L. Du, Z. Li, X. Yuan, *Light: Sci. Appl.* **2018**, *7*, 18001.
- [2] G.-Y. Lee, J.-Y. Hong, S. Hwang, S. Moon, H. Kang, S. Jeon, H. Kim, J.-H. Jeong, B. Lee, *Nat. Commun.* **2018**, *9*, 4562.
- [3] S. Lan, X. Zhang, M. Taghinejad, S. Rodrigues, K.-T. Lee, Z. Liu, W. Cai, *ACS Photonics* **2019**, *6*, 864.
- [4] J. Xiong, E.-L. Hsiang, Z. He, T. Zhan, S.-T. Wu, *Light: Sci. Appl.* **2021**, *10*, 216.
- [5] N. Meinzer, W. L. Barnes, I. R. Hooper, *Nat. Photonics* **2014**, *8*, 889.
- [6] J. Jang, G. Y. Lee, J. Sung, B. Lee, *Adv. Opt. Mater.* **2021**, *9*, 2100678.
- [7] Z. Li, C. Wan, C. Dai, J. Zhang, G. Zheng, Z. Li, *Adv. Opt. Mater.* **2021**, *9*, 2100297.
- [8] C. Wan, C. Dai, J. Zhang, S. Wan, Z. Li, G. Zheng, X. Zhang, Z. Li, *Small* **2021**, *17*, 2100561.
- [9] Z. Wang, C. Dai, Z. Li, Z. Li, *Nano Lett.* **2022**, *22*, 2059.
- [10] M. Khorasaninejad, Z. Shi, A. Y. Zhu, W.-T. Chen, V. Sanjeev, A. Zaidi, F. Capasso, *Nano Lett.* **2017**, *17*, 1819.
- [11] D. Wen, J. J. Cadusch, J. Meng, K. B. Crozier, *Adv. Funct. Mater.* **2020**, *30*, 1906415.
- [12] C. Wan, Z. Li, S. Wan, C. Dai, J. Tang, Y. Shi, Z. Li, *Adv. Funct. Mater.* **2021**, *32*, 2110592.
- [13] Q. Dai, Z. Guan, S. Chang, L. Deng, J. Tao, Z. Li, Z. Li, S. Yu, G. Zheng, S. Zhang, *Adv. Funct. Mater.* **2020**, *30*, 2003990.
- [14] H. Ren, X. Fang, J. Jang, J. Bürger, J. Rho, S. A. Maier, *Nat. Nanotechnol.* **2020**, *15*, 948.
- [15] M. Khorasaninejad, A. Ambrosio, P. Kanhaiya, F. Capasso, *Sci. Adv.* **2016**, *2*, e1501258.
- [16] Z. Wang, C. Dai, J. Zhang, D. Wang, Y. Shi, X. Wang, G. Zheng, X. Zhang, Z. Li, *Adv. Funct. Mater.* **2021**, *32*, 2110022.
- [17] Z. Li, M.-H. Kim, C. Wang, Z. Han, S. Shrestha, A. C. Overvig, M. Lu, A. Stein, A. M. Agarwal, M. Lončar, *Nat. Nanotechnol.* **2017**, *12*, 675.
- [18] S. Kim, D. A. Westly, B. J. Roxworthy, Q. Li, A. Yulaev, K. Srinivasan, V. A. Aksyuk, *Light: Sci. Appl.* **2018**, *7*, 72.
- [19] Y. Meng, Z. Liu, Z. Xie, R. Wang, T. Qi, F. Hu, H. Kim, Q. Xiao, X. Fu, Q. Wu, *Photonics Res.* **2020**, *8*, 564.
- [20] F. Ding, R. Deshpande, S. I. Bozhevolnyi, *Light: Sci. Appl.* **2018**, *7*, 17178.
- [21] L. Li, T. Li, X.-M. Tang, S.-M. Wang, Q.-J. Wang, S.-N. Zhu, *Light: Sci. Appl.* **2015**, *4*, e330.
- [22] S. Sun, Q. He, S. Xiao, Q. Xu, X. Li, L. Zhou, *Nat. Mater.* **2012**, *11*, 426.
- [23] R. Yang, Y. Shi, S. Wan, Z. Wang, Z. Li, J. *Lightwave Technol.* **2021**, *39*, 5558.
- [24] Z. Wang, T. Li, A. Soman, D. Mao, T. Kananen, T. Gu, *Nat. Commun.* **2019**, *10*, 3547.
- [25] R. Yang, Y. Shi, C. Dai, C. Wan, S. Wan, Z. Li, *Opt. Lett.* **2020**, *45*, 5640.
- [26] Y. Fan, X. L. Roux, A. Korovin, A. Lupu, A. de Lustrac, *ACS Nano* **2017**, *11*, 4599.
- [27] Y. Shi, R. Yang, C. Dai, C. Wan, Z. Li, *Opt. Lett.* **2022**, *47*, 369.
- [28] Y. Ha, Y. Guo, M. Pu, X. Li, X. Ma, Z. Zhang, X. Luo, *Adv. Theory Simul.* **2021**, *4*, 2000239.
- [29] J. Chen, T. Li, S. Wang, S. Zhu, *Nano Lett.* **2017**, *17*, 5051.
- [30] R. Singh, A. Agarwal, B. W. Anthony, *Sci. Rep.* **2020**, *10*, 19923.
- [31] X. Guo, Y. Ding, X. Chen, Y. Duan, X. Ni, *Sci. Adv.* **2020**, *6*, eabb4142.
- [32] Y. Ha, Y. Guo, M. Pu, F. Zhang, X. Li, X. Ma, M. Xu, X. Luo, *Opt. Express* **2020**, *28*, 7943.
- [33] A. Yulaev, W. Zhu, C. Zhang, D. A. Westly, H. J. Lezec, A. Agrawal, V. Aksyuk, *ACS Photonics* **2019**, *6*, 2902.
- [34] N. Zhou, S. Zheng, X. Cao, Y. Zhao, S. Gao, Y. Zhu, M. He, X. Cai, J. Wang, *Sci. Adv.* **2019**, *5*, eaau9593.
- [35] Z. Huang, D. L. Marks, D. R. Smith, *Opt. Express* **2019**, *27*, 35631.
- [36] Z. Huang, D. L. Marks, D. R. Smith, *Optica* **2019**, *6*, 119.
- [37] Z. Liu, C. Zhang, W. Zhu, Z. Huang, H. J. Lezec, A. Agrawal, L. J. Guo, *ACS Photonics* **2021**, *8*, 1112.
- [38] Z. Li, P. Lin, Y.-W. Huang, J.-S. Park, W. T. Chen, Z. Shi, C.-W. Qiu, J.-X. Cheng, F. Capasso, *Sci. Adv.* **2021**, *7*, eabe4458.
- [39] Z.-L. Deng, J. Deng, X. Zhuang, S. Wang, T. Shi, G. P. Wang, Y. Wang, J. Xu, Y. Cao, X. Wang, *Light: Sci. Appl.* **2018**, *7*, 78.